(Received 19 July 2024, Accepted 15 August 2024, Scheduled 30 August 2024)

Stator Winding InterTurn Short-Circuit Fault Detection in WRIM Using Rise and Fall Times of Stator Currents

Habachi Bilal[1, 2], Svetlana Dyagileva[2], Nicolas Heraud[2, *], Eric Jean Roy Sambatra[3], and Blaise Ravelo[4]

[1]*Laboratory of Electrical Engineering and Power Electronics, University of Lille, Arts et Metiers Institute of Technology Centrale Lille, Yncrea Hauts-de-France, ULR 2697-L2EP, F-59000 Lille, France*
[2]*Department of Renewable Energies-UMR CNRS 6134, University of Corsica, 20250, Corte*
[3]*Department of Industrial Engineering, Higher Institute of Technology (IST-D), Antsiranana, The Republic of Madagascar*
[4]*Nanjing University of Information Science & Technology (NUIST), School of Electronic & Information Engineering Nanjing 210044, Jiangsu, China*

ABSTRACT: One of the major challenges of today's rotating machine manufacturing industries is finding effective techniques to prevent early mechanical or electrical failure. Efficient troubleshooting methods must be developed for rotating electrical machines, such as three-phase and multiphase electrical induction or synchronous machines. A novel method for fault detection in a Wound Rotor Induction Machine (WRIM) is presented in this paper. Its originality lies in the determination of current rise and fall times in healthy and InterTurn short-Circuit Fault (ITSCF) cases. The method is based on using the two-current ($\mathbf{i_{sd}}$, $\mathbf{i_{sq}}$) sigmoid transform (ST) of Park's vector approach. A WRIM with a nominal power of 0.3 kW is used for the analytical and experimental studies. The type of fault detection being studied is short circuit InterTurns on one phase of the stator winding. The results are promising because the methodology used is simple, fast, and accurate for diagnosing this type of fault, and can detect a low number of short-circuit InterTurns in the stator winding.

1. INTRODUCTION

Numerous methodologies exist for detecting or identifying electrical faults in Wound Rotor Induction Machine WRIM or Doubly Fed Induction Machine (DFIM). Implementing these approaches is crucial for detecting failures promptly, preventing unplanned downtime, and ultimately mitigating economic losses. Several studies have been undertaken to detect or identify InterTurn Short-Circuit Fault (ITSCF) occurring in both the rotor and stator windings of induction machines, whether they are equipped with wound rotors or designed as induction machines. For the stator, many studies have been performed to diagnose short-circuit faults. In fact, the authors of [1] proposed a method for the early detection and localization of an ITSCF in the stator winding of an induction motor. They used the Discrete Wavelet Energy Ratio (DWER) of three stator currents and Artificial Neural Network (ANN) for diagnosis. In [2], a Sweep Frequency Response Analysis (SFRA) method was proposed for detecting the ITSCF in a stator winding. However, with the proposed method, the authors are unable to quantify the defect under study. The use of ESLF (End-Shield Leakage Fluxes) has been proposed in [3] and investigated the detection of InterTurn short-circuit faults in the stator winding of an asynchronous machine. With ESLF, the authors noted that the proposed fault indicator was independent of the number of poles and the location of the fault in one of the stator windings. In [4], a general fault diagnosis method was presented and applied to faults in the stator and rotor windings of a WRIM. This identification method is based on Feature-bilateral flux Linkage Difference Vector (FLDV) which is the difference between the flux calculated by the current model and the flux calculated by the voltage model. To diagnose the ITSCF in the stator winding of a WRIM, Deep Learning was used in [5–10]. The authors in [11–16] have worked on the wavelet transform for diagnosing the ITSCF in the stator winding of a WRIM. Refs. [17] and [18] proposed a technique using a genetic algorithm for detection and localization in the initial phase of an ITSCF in an Induction Machine (IM). A technique based on V-I (Voltage-Current) was proposed in [19] and [20]. This technique allowed them to detect and locate the ITSCF in the stator winding of an IM. In [21] and [22], the authors proposed an artificial intelligence ANN to detect short-circuit faults in the stator windings of an IM. With ANN, their method was unable to quantify the number of short-circuit turns. Kalman filter was used in [23] as a technique for detecting the ITSCF in the stator winding of an IM. In another work, Motor Current Signal Analysis (MCSA) was proposed by the authors in [13, 24, 25] to detect the fault of an ITSC in the windings of a WRIM and an IM. A technique based on an empirical method was proposed in [26]. In [11, 27, 28] a technique based on the Fourier transform and least squares analysis of Park vectors was developed. Using the latter, the authors in [28] were able to quantify the short-circuit fault in the stator winding of a DFIM.

Regarding the various techniques mentioned above, such as the Wavelet Transform and MCSA, the authors in [29] asserted that the use of these conventional methods often serves only to detect certain types of known anomalies and is thus unable to detect any new abnormal behavior present in the system.

* Corresponding author: Nicolas Heraud (heraud@univ-corse.fr).

In addition, if the spectrum of a healthy WRIM is close to or overlapping with that of a faulty WRIM, it is difficult to distinguish faulty from healthy operating conditions. Techniques based on Artificial Intelligence (AI) are known for their performance, but they depend on a large amount of data, which leads to large computations in the learning process, making these algorithms relatively complex [30]. In practice, there are many cases where the severity of a short-circuit fault between windings must be estimated with a high degree of diagnostic accuracy. This paper develops an approach for detecting ITSCF in the winding of a WRIM. It is a particularly simple and fast fault detection method. A noninvasive approach based on Park's Vector Approach (PVA) and the sigmoid function is proposed. The involved calculations are very simple in the presented work, unlike Motor Current Signal Analysis (MCSA) methods, which require frequency analysis of the signals or ANN methods, which need heavy computation time. Its method is not sensitive to harmonics present on the electrical network but remains sensitive in noisy current measurements case. The currents on the three stator phases (I_{sA}, I_{sB}, and I_{sC}) become two currents (i_{sd} and i_{sq}) in the Park vector approach. The sigmoid function is then applied to the two currents (i_{sd} and i_{sq}). Using the sigmoid function on the two currents (i_{sd} and i_{sq}), one can easily obtain the rise time (R_t), fall time (F_t) and their offsets. These two parameters (R_t) and F_t) are used to detect short-circuits and quantify their severity. To achieve this, the second section is dedicated to modeling the DFIM with or without the ITSC in the stator windings. The third section describes the experimental study, test bench, and temporal currents. The analysis of the two times leads to the fourth section and allows us to detect and quantify the ITSCF. A comparison between the performance of the developed method and that in the literature is discussed. Finally, Section 5 provides the conclusion.

2. HEALTHING AND FAULTY CONDITIONS ANALYSIS USING THE WRIM MODEL

The details of the various steps involved in the developed detection method and quantification are shown in Fig. 1.

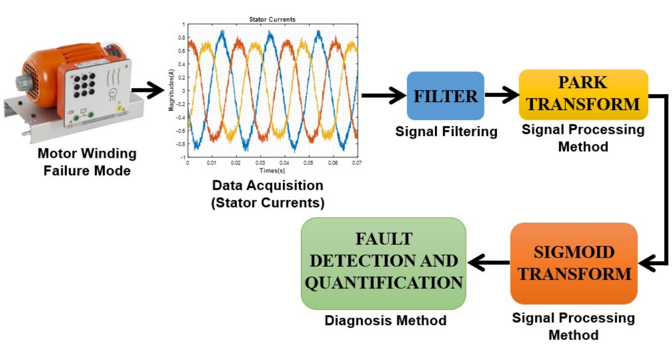

FIGURE 1. Steps for detecting ITSCF.

The stator windings of the WRIM in a healthy state are shown in Fig. 3. The numbers of stator windings for the three phases (phase "A", phase "B", and phase "C") are N_{sA}, N_{sB}, and N_{sC}, respectively. I_{sA}, I_{sB}, and I_{sC} are the three stator currents (WRIM model or experimental). If phase "A" is affected by the short-circuit fault, I_{sA} becomes I_{sA1}. V_{sA}, V_{sB}, and V_{sC} are the three stator voltages. However, Fig. 3 shows the stator winding where one of the phases is subject to the ITSCF. As in the healthy case, N_{sB} and N_{sC} are the number of turns on the "B" phases. Then, N_{sA1} is the number of reduced turns on phase "A", and N_{sA2} is the shortened part. I_{sA2} is the current in this shorted part. In the two illustrations, Fig. 2 and Fig. 3, the difference lies in the winding structure since in the defective case the winding of phase "A" is no longer symmetrical concerning the other two phases. The non-symmetric nature of phase "A" leads to an increase in the size of the vectors (voltage vector and current vector) and matrices (resistance and inductance matrices) that characterize the WRIM model. For WRIM modeling, various equations are quoted from the authors' previous work [31].

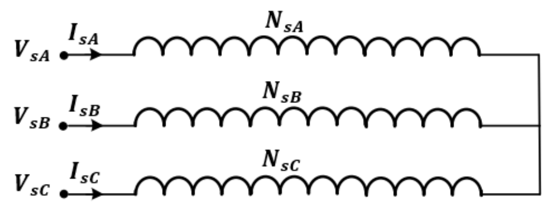

FIGURE 2. Stator winding representation healthy state.

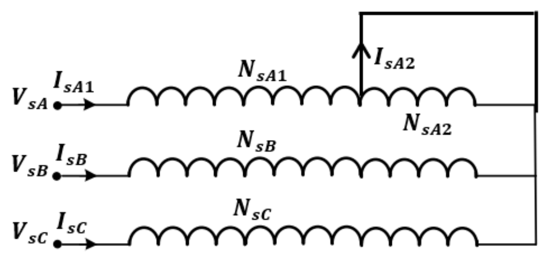

FIGURE 3. Stator winding representation with the ITSCF in phase "A".

3. EXPERIMENTAL STUDY AND PRESENTATION OF THE THREE STATOR CURRENTS

3.1. Test Bench Presentation

In the present study, WRIM currents are recorded from measurements. The sampling frequency is 20 kHz. The fault is in phase "A" (the first stator phase).

The various devices shown in Fig. 4 are described as follows:

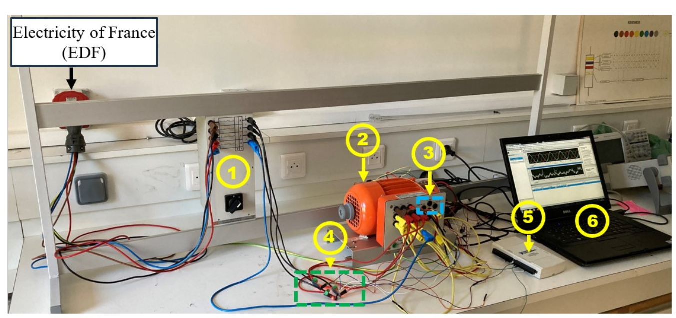

FIGURE 4. Test bench.

1. WRIM power supply box,
2. WRIM,
3. Short-circuit terminal,
4. Current sensors,
5. Acquisition card (NI-USB6218),
6. Computer.

The three phases of the WRIM stator contain six coils in series. In addition, each coil has 133 turns for a total of 798 turns in series. The test bench includes an induction machine with a wound rotor, a sensor that measures the machine currents, an acquisition card, and a computer for data processing.

TABLE 1. Features of the WRIM.

Specifications	Values	Units
Rated frequency, f_n	50	Hz
Rated voltage, U_n ($\triangle$/Y)	230/400	V
Rated power, P_n	0.3	kW
Rated speed, V_n	1488	rpm
Rated current, I_n ($\triangle$/Y)	1.5/0.87	A
Number of pole pairs, p	2	-

For this purpose, the features of the WRIM are presented in Table 1. The short-circuit turn ratios (R_{sh}) used in this study are shown in Table 2.

TABLE 2. InterTurn Short-Circuit Fault.

Number of short-circuit turns (N_{sh})	R_{sh}(%)
20	2.5
40	5
80	10
160	20
240	30
320	40

The configuration of the ITSCF is shown in Fig. 3. This test bench (Fig. 4) can be used to simulate different conditions: healthy state and in the presence of an ITSCF. To calculate R_{sh}(%), the relationship is as follows:

$$R_{sh}(\%) = \frac{N_{sh}}{N_s} \times 100 \qquad (1)$$

where N_s is the total number of turns on a phase.

3.2. The Three Currents of the WRIM Model and Experiment

Both Fig. 5 and Fig. 6 show the three currents from the three phases of the WRIM stator in the healthy case and in the presence of the ITSCF. In the fault case, the greater the number of short circuits is, the greater the amplitudes of phase "A" is. However, the deformations and changes in current amplitudes in phases "B" and "C" are phenomena related to the short-circuit fault in phase "A" of the WRIM stator.

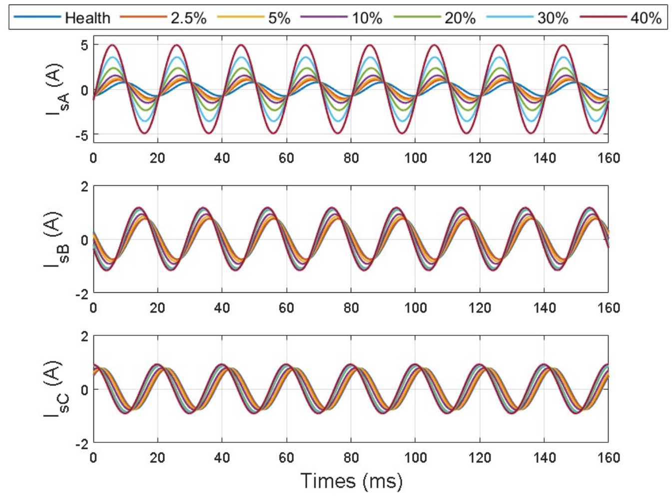

FIGURE 5. Three-phase currents from the stator in both cases (healthy and faulty): WRIM model.

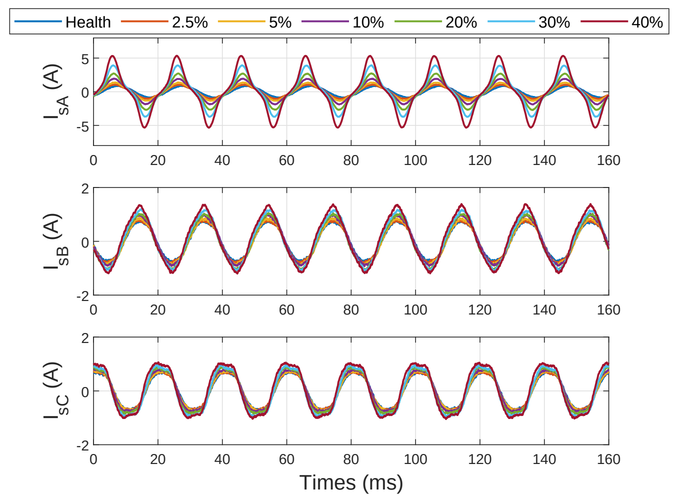

FIGURE 6. Three-phase currents from the stator in both cases (healthy and faulty): experimental part.

4. PARK'S VECTOR APPROACH AND SIGMOID TRANSFORM

4.1. PVA

PVA is a technique introduced by Marques Cardoso et al. in 1999, as described in [32] and later extended to multiple fault diagnosis in the IM and WRIM. This technique combines the information of three-phase currents into two equivalent currents in the reference frame obtained by the transformation. The PVA is represented by [32–34]:

$$\begin{cases} i_{sd} = \sqrt{\frac{2}{3}} I_{sA} - \frac{1}{\sqrt{6}} I_{sB} - \frac{1}{\sqrt{6}} I_{sC} \\ i_{sq} = \frac{1}{\sqrt{2}} I_{sB} - \frac{1}{\sqrt{2}} I_{sC} \end{cases} \qquad (2)$$

The two currents i_{sd} and i_{sq} are then used in the sigmoid function to obtain R_t and F_t for fault detection.

4.2. Sigmoid Transform

The main idea of this work is to apply ST to two PVA currents i_{sd} and i_{sq}. This function is used to obtain R_t and F_t. Then, the i_{sd} and i_{sq} currents are normalized using the ST so that the fault diagnosis method is not affected by variations in load torque and motor speed in the three phases (I_{sA}, I_{sB}, and I_{sC}). The ST of the real variable x is defined as follows: where λ is a positive real. Fig. 7 shows the sigmoid function of the sinusoidal variable x. $F(x)$ varies from 0 to 1 and has the same period as the variable x. The effect of positive real λ on the dynamics of $F(x)$ is shown in Fig. 7. The greater the λ is, the faster the $F(x)$ changes.

$$F(x) = \frac{1}{1 + e^{-\lambda x}} \tag{3}$$

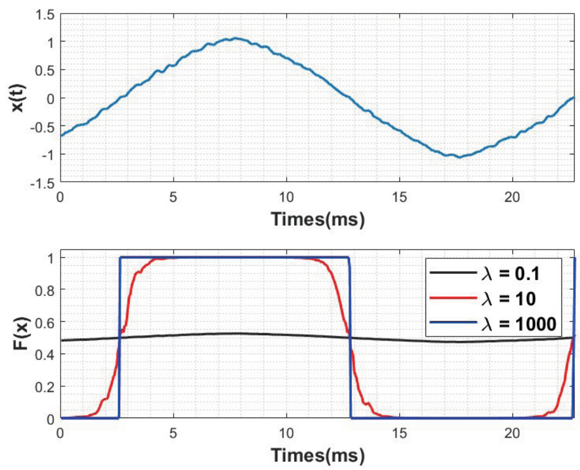

FIGURE 7. Sigmoid function for different coefficient values λ.

Using (2) and (3), we obtain Fig. 8, Fig. 9, Fig. 10, and Fig. 11. These four figures show the effect of a short-circuit fault between the windings of phase "A" and the other two phases (B and C) of the WRIM stator winding.

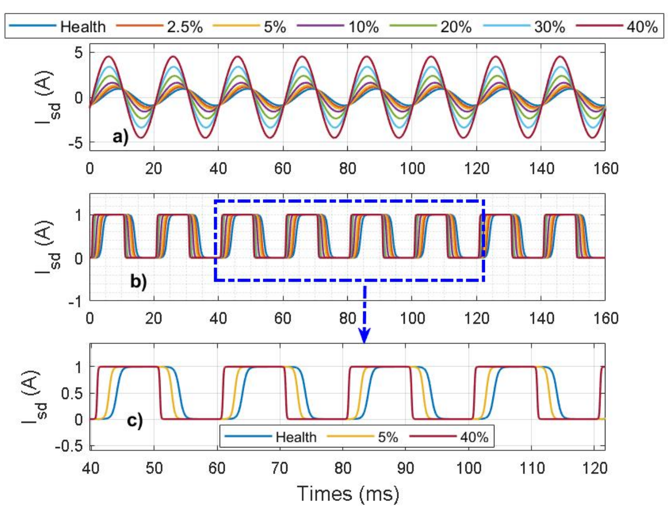

FIGURE 8. WRIM model: (a) i_{sd} currents, (b) i_{sd} currents from ST and (c) zoom.

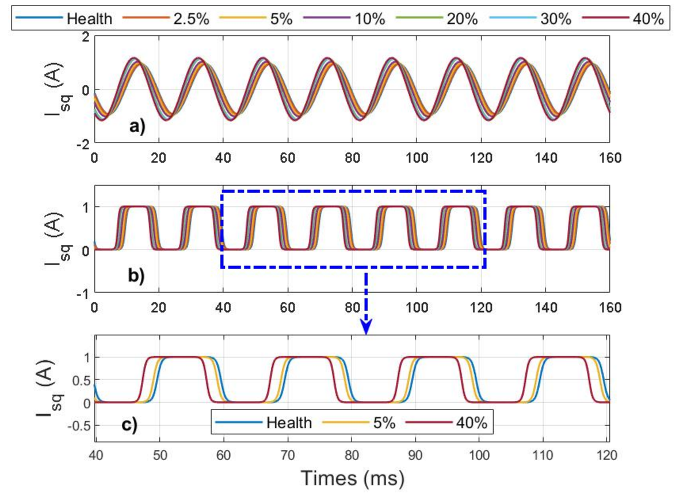

FIGURE 9. WRIM model: (a) i_{sq} currents, (b) i_{sq} currents from ST and (c) zoom.

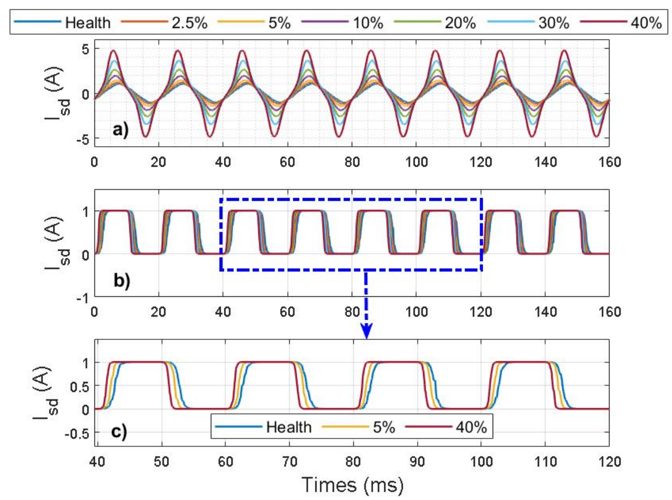

FIGURE 10. Experimental part: (a) i_{sd} currents, (b) i_{sd} currents from ST and (c) zoom.

Figures 10 and 11 show that there are shifts between the i_{sd} currents without the presence of InterTurn short-circuit fault. Similarly, there are some offsets for i_{sq} currents, but not too much compared to i_{sd} currents. The offsets result from the rise and fall times of each change in the rate of shortened windings in phase "A" of the stator.

5. DISPLAY OF R_t, F_t AND THEIR OFFSETS

5.1. Rise Time R_t and Fall Time F_t

Before presenting the R_t and F_t values of i_{sd} and i_{sq} currents, let us see how these two parameters are calculated:

- R_t is calculated between 10% and 90% of the signal variation. Let T_1 and T_2 be the times when the response reaches 10% and 90% of its final value, respectively (see Fig. 12).
- F_t is calculated between 90% and 10% of the signal variation. Let T_3 and T_4 be the times when the response reaches 90% and 10% of its final value, respectively (see Fig. 12).

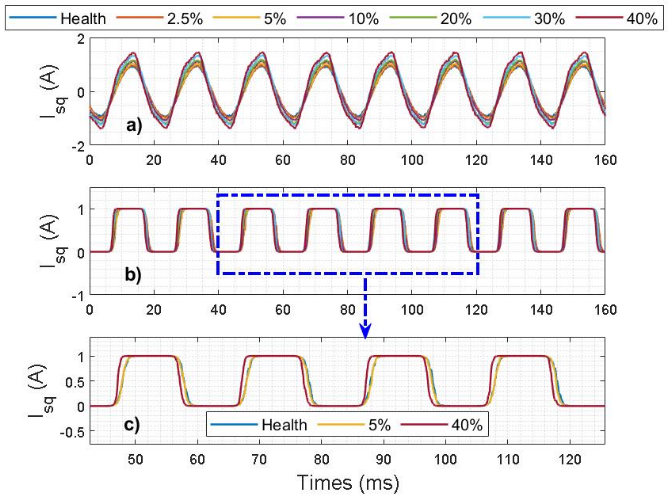

FIGURE 11. Experimental part: (a) i_{sq} currents, (b) i_{sq} currents from ST and (c) zoom.

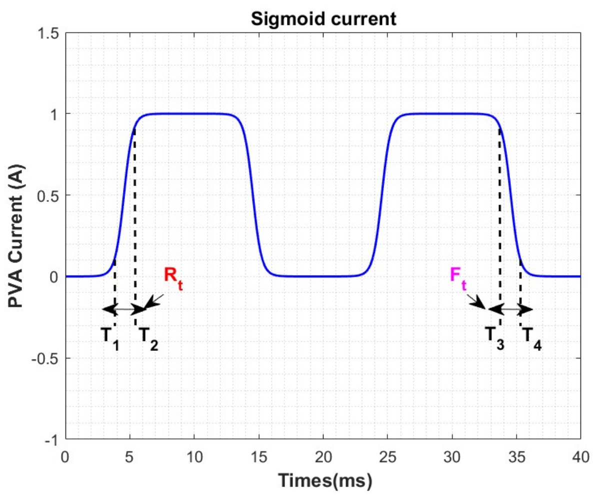

FIGURE 12. Methods for obtaining the rise and fall times (R_t and F_t).

T_1, T_2, T_3, and T_4 are the averages of the rising and falling edge times observed for 160 ms. The equations to obtain R_t and F_t are (4) and (5):

$$R_t = T_{2(90\%)} - T_{1(10\%)} \tag{4}$$

$$F_t = T_{4(10\%)} - T_{3(90\%)} \tag{5}$$

Table 3 and Table 4 summarize the values for the rise and fall times of the i_{sd} and i_{sq} currents. They show how the Inter-Turn short-circuits fault influences the rise time and fall time of i_{sd} and i_{sq} currents, since they evolve according to the ratio of the short-circuit turns. These values show small changes in R_t and F_t, which are normal since the fault is not in i_{sq} (see (2)). Eventually, R_t and F_t are the same in the faulty case and in the healthy case. Then, as the number of shorted windings increases, R_t or F_t of the faulty case decreases compared to that of the healthy case.

5.2. Offset for R_t and F_t

This section shows the current offset values. The current offset is used to detect and quantify InterTurn short circuit faults. As a result, the method for obtaining the R_t or F_t offset between the healthy and faulty cases is shown in Fig. 13. In the latter, the offsets are calculated as:

$$D_{R_t} = R_{t(Health)} - R_{t(Fault)} \tag{6}$$

$$D_{F_t} = F_{t(Health)} - F_{t(Fault)} \tag{7}$$

where D_{R_t} and D_{F_t} are the offsets from R_t and F_t respectively.

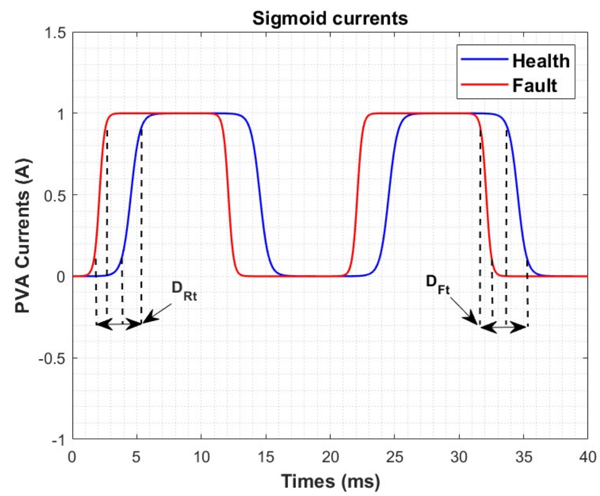

FIGURE 13. Method of obtaining the offset from R_t or F_t.

The current offset values for the theoretical and experimental cases are shown in Table 5 and Table 6. As a result, these values indicate that as the number of short-circuit windings increases, the offset of the currents (i_{sd} and i_{sq}) in the presence of the fault changes concerning the healthy current. Compared to the two PVA currents, the offset evolutions are more significant in i_{sd} than in i_{sq}.

Then, D_{R_t} and D_{F_t} will show the same evolution values. Therefore, only D_{R_t} is taken into account when modeling offset trends, and the different D_{R_t} models are written from i_{sd} and i_{sq} streams. Fig. 14 illustrates the D_{R_t} models derived from the i_{sd} current in the theoretical and experimental cases. Fig. 15 illustrates the patterns of D_{R_t} derived from the i_{sq} current in the theoretical and experimental cases. This gives us two models derived from the offset of the two PVA currents. These two Equations (8) and (9) show that the ITSCF can be detected from the rise or fall time offset of the currents derived from the sigmoid function. Then, the two models expressed by Equations (8) and (9) are obtained via the method of least squares.

The evolution of D_{R_t} models (theoretical and experimental cases) gives a logarithmic model of the following form:

$$D_{R_t}(R_{sh}) = p_2 \log(1 + p_1 R_{sh}). \tag{8}$$

where p_1 and p_2 are two constants of the two models shown in Fig. 14. Here are the values of the two constants:

TABLE 3. Theoretical case study.

R_{sh} (%)	T_1 (ms)		T_2 (ms)		R_t (ms)		T_3 (ms)		T_4 (ms)		F_t (ms)	
	for i_{sd}	for i_{sq}	for i_{sd}	for i_{sq}	for i_{sd}	for i_{sq}	for i_{sd}	for i_{sq}	for i_{sd}	for i_{sq}	for i_{sd}	for i_{sq}
0	73.30	78.80	74.80	80.30	1.50	1.50	83.30	88.80	84.80	90.30	1.50	1.50
2.5	72.70	78.60	73.90	80.10	1.20	1.50	82.70	88.60	83.90	90.10	1.20	1.50
5	72.25	78.27	73.35	79.70	1.10	1.43	82.25	88.22	83.35	89.65	1.10	1.43
10	71.65	77.75	72.55	79.10	0.90	1.35	81.65	87.75	82.55	89.10	0.90	1.35
20	71.10	77.15	71.70	78.40	0.60	1.25	81.10	87.15	81.70	88.40	0.60	1.25
30	70.85	76.94	71.30	78.10	0.45	1.16	80.85	86.94	81.30	88.10	0.45	1.16
40	70.78	76.79	71.08	77.85	0.30	1.06	80.78	86.79	81.08	87.85	0.30	1.06

TABLE 4. Experimental case study.

R_{sh} (%)	T_1 (ms)		T_2 (ms)		R_t (ms)		T_3 (ms)		T_4 (ms)		F_t (ms)	
	for i_{sd}	for i_{sq}	for i_{sd}	for i_{sq}	for i_{sd}	for i_{sq}	for i_{sd}	for i_{sq}	for i_{sd}	for i_{sq}	for i_{sd}	for i_{sq}
0	72.00	77.16	73.35	78.66	1.50	1.50	82.00	87.16	83.50	86.66	1.50	1.50
2.5	71.68	77.19	72.92	78.69	1.24	1.50	81.85	87.23	83.09	88.73	1.24	1.50
5	71.46	77.21	72.64	78.68	1.18	1.46	81.47	87.12	82.64	88.58	1.18	1.46
10	71.33	76.98	72.41	78.43	1.08	1.45	81.40	86.98	82.48	88.43	1.08	1.45
20	71.27	76.74	72.20	78.06	0.93	1.32	81.27	86.74	82.20	88.06	0.93	1.32
30	71.09	76.67	71.87	77.85	0.78	1.18	81.28	86.63	82.06	87.80	0.78	1.18
40	71.00	76.64	71.69	77.73	0.69	1.09	81.00	86.64	81.69	87.73	0.69	1.09

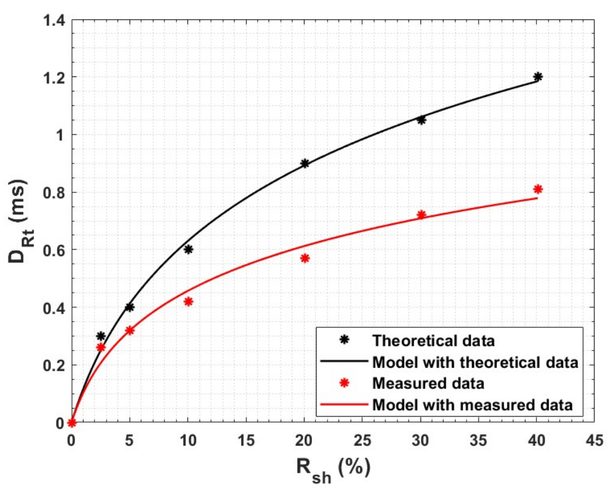

FIGURE 14. D_{R_t} models from the i_{sd} current.

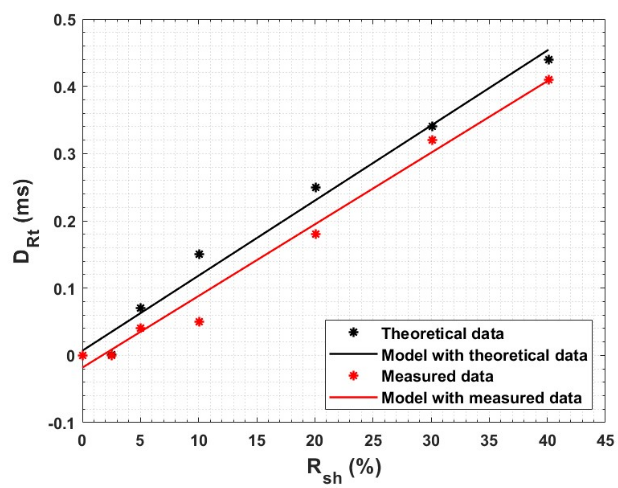

FIGURE 15. D_{R_t} models from the i_{sq} current.

The evolution of D_{R_t} (theoretical and experimental cases) gives a linear model of the following form:

$$D_{R_t}(R_{sh}) = p_3 R_{sh} + p_4. \tag{9}$$

where p_3 and p_4 are two constants of the two models shown in Fig. 15. Here are the values of the two constants:

The measurement, shown by red point in Fig. 16, corresponding to $R_{sh} = 10\%$, is $D'_{R_t} = 0.42$. As shown on Fig. 16, the model, obtained by Equation (8) gives $R_{sh} = 8.42\%$ for $D'_{R_t} = 0.42$. The error between these two values is about 20% which is quite acceptable, bearing in mind that this point is quite unfavorable, as it is the one farther from the modeled curve. A similar study can be done on Fig. 17. The measurement spotted by red point for $R_{sh} = 10\%$ is $D'_{R_t} = 0.05$. From this value, the model given by (9) permits to deduce $R_{sh} = 7\%$ which corresponds to an error of 30%. Therefore, this model should be essentially used to confirm an ITSC defect.

TABLE 5. Theoretical case study.

i_{sd}	D_{R_t} (ms)	D_{F_t} (ms)	i_{sq}	D_{R_t} (ms)	D_{F_t} (ms)
D_1	0.30	0.30	D_1	0	0
D_2	0.40	0.40	D_2	0.07	0.07
D_3	0.60	0.60	D_3	0.15	0.15
D_4	0.90	0.90	D_4	0.25	0.25
D_5	1.05	1.05	D_5	0.34	0.34
D_6	1.20	1.20	D_6	0.44	0.44

TABLE 6. Experimental case study.

i_{sd}	D_{R_t} (ms)	D_{F_t} (ms)	i_{sq}	D_{R_t} (ms)	D_{F_t} (ms)
D_1	0.26	0.26	D_1	0	0
D_2	0.32	0.32	D_2	0.04	0.04
D_3	0.42	0.42	D_3	0.05	0.05
D_4	0.57	0.57	D_4	0.18	0.18
D_5	0.72	0.72	D_5	0.32	0.32
D_6	0.81	0.81	D_6	0.41	0.41

TABLE 7. Values of the two model constants.

Studies	p_1	p_2
Theoretical	0.476	0.276
Measurement	0.493	0.253

TABLE 8. Values of the two model constants.

Studies	p_3	p_4
Theoretical	0.0117	0.0069
Measurement	0.0108	−0.0234

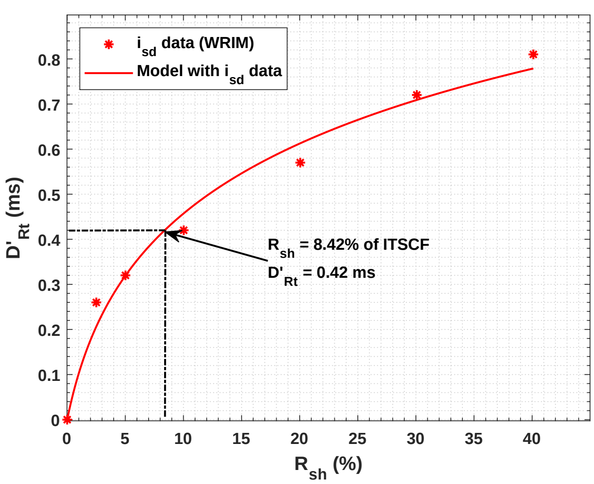

FIGURE 16. D'_{R_t} projections from PVA (i_{sd}).

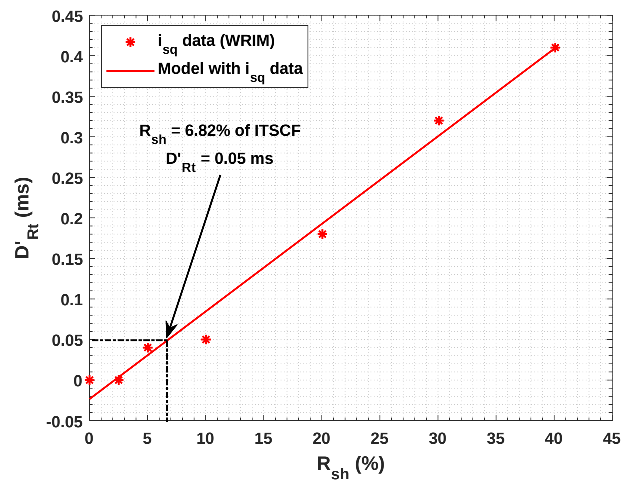

FIGURE 17. D'_{R_t} projections from PVA (i_{sq}).

6. CONCLUSION

This paper presents a new methodology for detecting short-circuit faults in DFIM and for evaluating the evolution of these faults, based on the two-current ST of the PVA. The evolution of defects since their appearance is studied. Diagnosis takes full advantage of the offset time of the currents generated by the sigmoid function. In fact, the current offset times evolve according to the severity of the fault. When the number of short-circuit turns increases (2.5% to 40%), the rise and fall times of the currents are earlier than those in the healthy case. With the present study, it is possible to quantify the number of shorted turns in the WRIM winding with good accuracy. It can also be used to detect short-circuit faults on electric vehicles motors or generators installed in wind farms. This simplicity of calculation makes it possible to monitor ITSCF in real time. This method, which does not use conventional methods (MCSA) for detecting ITSCF, provides detection redundancy and it is a valuable complement to the others.

REFERENCES

[1] Cherif, H., A. Benakcha, I. Laib, S. E. Chehaidia, A. Menacer, B. Soudan, and A. G. Olabi, "Early detection and localization of stator inter-turn faults based on discrete wavelet energy ratio and neural networks in induction motor," *Energy*, Vol. 212, 118684, Dec. 2020.

[2] Ranzinger, L., S. Uhrig, and S. Tenbohlen, "Analysis and modeling the frequency response of rotating machines regarding fault diagnosis using SFRA," *IEEE Transactions on Energy Conversion*, Vol. 39, No. 1, 747–756, 2023.

[3] Athikessavan, S. C., E. Jeyasankar, and S. K. Panda, "Inter-turn fault detection of induction motors using end-shield leakage fluxes," *IEEE Transactions on Energy Conversion*, Vol. 37, No. 4, 2260–2270, Dec. 2022.

[4] Fu, Y., Z. Ren, S. Wei, Y. Xu, and F. Li, "Using flux linkage difference vector in early inter-turn short circuit detection for the windings of offshore wind DFIGs," *IEEE Transactions on Energy Conversion*, Vol. 36, No. 4, 3007–3015, Dec. 2021.

[5] Nazemi, M., X. Liang, and F. Haghjoo, "Convolutional neural network-based online stator inter-turn faults detection for line-connected induction motors," *IEEE Transactions on Industry Applications*, Vol. 60, No. 3, 4693–4707, 2024.

[6] Husari, F. and J. Seshadrinath, "Stator turn fault diagnosis and severity assessment in converter-fed induction motor using flat diagnosis structure based on deep learning approach," *IEEE Journal of Emerging and Selected Topics in Power Electronics*, Vol. 11, No. 6, 5649–5657, Dec. 2023.

[7] Alipoor, G., S. J. Mirbagheri, S. M. M. Moosavi, and S. M. A. Cruz, "Incipient detection of stator inter-turn short-circuit faults in a doubly-fed induction generator using deep learning," *IET Electric Power Applications*, Vol. 17, No. 2, 256–267, 2023.

[8] Husari, F. and J. Seshadrinath, "Early stator fault detection and condition identification in induction motor using novel deep network," *IEEE Transactions on Artificial Intelligence*, Vol. 3, No. 5, 809–818, Oct. 2022.

[9] Attallah, O., R. A. Ibrahim, and N. E. Zakzouk, "Fault diagnosis for induction generator-based wind turbine using ensemble deep learning techniques," *Energy Reports*, Vol. 8, 12 787–12 798, Nov. 2022.

[10] Husari, F. and J. Seshadrinath, "Sensitive inter-tum fault identifcation in induction motors using deep learning based methods," in *2020 IEEE International Conference on Power Electronics, Smart Grid and Renewable Energy (PESGRE2020)*, 1–6, Cochin, India, Jan. 2020.

[11] Indiran, R. R. and A. A. Stonier, "Inter-turn short-circuit faults detection and monitoring of induction machines using WPT-fuzzy logic approach based on online condition," *Journal of Circuits, Systems and Computers*, Vol. 32, No. 01, 2350001, 2023.

[12] Saucedo-Dorantes, J. J., A. Y. Jaen-Cuellar, A. Perez-Cruz, and D. A. Elvira-Ortiz, "Detection of inter-turn short circuits in induction motors under the start-up transient by means of an empirical wavelet transform and self-organizing map," *Machines*, Vol. 11, No. 10, 958, Oct. 2023.

[13] Hamatwi, E., P. Barendse, and A. Khan, "An investigation into the diagnosis of interturn winding faults in a scaled-down DFIG using the MCSA and DWT of the stator and rotor current," in *2021 IEEE Energy Conversion Congress and Exposition (ECCE)*, 3797–3804, Vancouver, BC, Canada, Oct. 2021.

[14] Hussein, A. M., A. A. Obed, R. H. A. Zubo, Y. I. A. Al-Yasir, A. L. Saleh, H. Fadhel, A. Sheikh-Akbari, G. Mokryani, and R. A. Abd-Alhameed, "Detection and diagnosis of stator and rotor electrical faults for three-phase induction motor via wavelet energy approach," *Electronics*, Vol. 11, No. 8, 1253, Jan. 2022.

[15] Almounajjed, A. and A. K. Sahoo, "Wavelet-based multi-class support vector machine for stator fault diagnosis in induction motor," *Transactions of the Institute of Measurement and Control*, Vol. 45, No. 2, 261–273, 2023.

[16] Akhil Vinayak, B., K. A. Anand, and G. Jagadanand, "Wavelet-based real-time stator fault detection of inverter-fed induction motor," *IET Electric Power Applications*, Vol. 14, No. 1, 82–90, 2020.

[17] Aswad, R. A. K. and B. M. H. Jassim, "Detection and localization of the stator winding inter-turn fault in induction motors based on parameters estimation using genetic algorithm," *Journal of the Institution of Engineers (India): Series B*, Vol. 103, No. 2, 405–414, 2022.

[18] Tomczyk, M., R. Mielnik, A. Plichta, I. Gołdasz, and M. Sułowicz, "Application of genetic algorithm for inter-turn short circuit detection in stator winding of induction motor," *Energies*, Vol. 14, No. 24, 8523, 2021.

[19] Dongare, U., B. Umre, and M. Ballal, "Stator inter-turn short-circuit fault diagnosis in induction motors applying VI loci-based technique," *Energy Reports*, Vol. 9, 1483–1493, Oct. 2023.

[20] Dongare, U. V., B. S. Umre, and M. S. Ballal, "Voltage-current locus-based stator winding inter-turn fault detection in induction motors," *International Journal of Circuit Theory and Applications*, Vol. 51, No. 6, 2889–2911, 2023.

[21] Noussaiba, L. A. E. and F. Abdelaziz, "ANN-based fault diagnosis of induction motor under stator inter-turn short-circuits and unbalanced supply voltage," *ISA Transactions*, Vol. 145, 373–386, 2024.

[22] Rajamany, G., S. Srinivasan, K. Rajamany, and R. K. Natarajan, "Induction motor stator interturn short circuit fault detection in accordance with line current sequence components using artificial neural network," *Journal of Electrical and Computer Engineering*, Vol. 2019, No. 1, 4825787, Dec. 2019.

[23] Namdar, A., H. Samet, M. Allahbakhshi, M. Tajdinian, and T. Ghanbari, "A robust stator inter-turn fault detection in induction motor utilizing kalman filter-based algorithm," *Measurement*, Vol. 187, 110181, Jan. 2022.

[24] Prakash, R. B. R., M. r. Ranga, A. Pandian, and P. S. Varma, "Induction machine stator winding failure detection using motor current signature analysis," in *IOP Conference Series: Materials Science and Engineering*, Vol. 993, No. 1, 012084, 2020.

[25] Saied, B. and A. J. Ali, "Fault prediction of deep bar cage rotor induction motor based on FEM," *Progress In Electromagnetics Research B*, Vol. 53, 291–314, 2013.

[26] Rehman, A. U., Y. Chen, G. Huang, Y. Yang, S. Wang, Y. Zhao, Y. Zhao, Y. Cheng, and T. Tanaka, "Stator inter-turns short circuit fault detection in DFIG using empirical mode decomposition method on leakage flux," in *2020 International Conference on Sensing, Measurement & Data Analytics in the Era of Artificial Intelligence (ICSMD)*, 184–187, Xi'an, China, Oct. 2020.

[27] Ghanbari, T. and A. Mehraban, "Stator winding fault detection of induction motors using fast Fourier transform on rotor slot harmonics and least square analysis of the Park's vectors," *IET Electric Power Applications*, Vol. 18, No. 3, 356–366, 2024.

[28] Bilal, H., N. Heraud, and E. J. R. Sambatra, "An experimental approach for detection and quantification of short-circuit on a doubly fed induction machine (DFIM) windings," *Journal of Control, Automation and Electrical Systems*, Vol. 32, No. 4, 1123–1130, 2021.

[29] Xu, Z., C. Hu, F. Yang, S.-H. Kuo, C.-K. Goh, A. Gupta, and S. Nadarajan, "Data-driven inter-turn short circuit fault detection in induction machines," *IEEE Access*, Vol. 5, 25 055–25 068, 2017.

[30] Chen, X., P. Qin, Y. Chen, J. Zhao, W. Li, Y. Mao, and T. Zhao, "Inter-turn short circuit fault diagnosis of PMSM," *Electronics*, Vol. 11, No. 10, 1576, 2022.

[31] Bilal, H., E. J. Sambatra, N. Heraud, J.-M. Razafimahenina, and S. Dyagileva, "Detection of inter-turn short-circuit on a doubly fed induction machine with dq axis representation-application to different power levels," *Progress In Electromagnetics Research B*, Vol. 95, 23–40, 2022.

[32] Marques Cardoso, A. J., S. M. A. Cruz, and D. S. B. Fonseca, "Inter-turn stator winding fault diagnosis in three-phase induction motors, by Park's vector approach," *IEEE Transactions on Energy Conversion*, Vol. 14, No. 3, 595–598, Sep. 1999.

[33] Parra, A. P., M. C. A. Enciso, J. O. Ochoa, and J. A. P. Peñaranda, "Stator fault diagnosis on squirrel cage induction motors by ESA and EPVA," in *2013 Workshop on Power Electronics and Power Quality Applications (PEPQA)*, 1–6, Bogota, Colombia, Jul. 2013.

[34] Cruz, S. M. A. and A. J. M. Cardoso, "Stator winding fault diagnosis in three-phase synchronous and asynchronous motors, by the extended Park's vector approach," *IEEE Transactions on Industry Applications*, Vol. 37, No. 5, 1227–1233, Sep.-Oct. 2001.